

Article

Experimental Study to Replicate Wood Fuel Conversion in a Downdraft Gasifier: Features and Mechanism of Single Particle Combustion in an Inert Channel

Denis Svishchev

Laboratory of Thermodynamics, Melentiev Energy Systems Institute of Siberian Branch of the Russian Academy of Sciences, 130 Lermontov Street, 664033 Irkutsk, Russia; denis.svishchev@gmail.com

Abstract: Downdraft gasification is a promising process of energy conversion of wood biomass. There are such fuel conversion conditions that differ favorably from conventional conditions. In such conditions, there is no pyrolysis zone in the fuel bed, which precedes the oxidation zone. Fuel is supplied into the oxidizing zone without charring, where it reacts with the intensive cold air flow from tuyeres. The study aims to replicate the conversion of particles in a gasifier close to tuyeres. For this purpose, the individual particles are burned in the muffle furnace space and the quartz channel replicating presence of other bed particles at a first approximation. In the experiment, the furnace temperature was varied, as well as the velocity of air supplied to the particle. Two-stage and single-stage mechanisms of particle combustion were identified. A two-stage process is observed in the range of tuyere velocities below 20 m s^{-1} . The two-stage mechanism is characterized by a stage of devolatilization and volatiles combustion, followed by a stage of char residue combustion. The stages are predominantly separate from each other, and their degree of overlapping is low, amounting to 24%. At the tuyere velocities above 125 m s^{-1} combustion of particles is realized primarily as a single-stage process. The intensive air flow reaches the fuel particle surface and initiates combustion of the surface char layer. In this case, the stages of devolatilization and char residue combustion run concurrently for the most part. In the single-stage mechanism, the degree of stage overlapping is significantly higher and amounts to 60–95%. For the two-stage combustion mechanism, the effect of cyclic movement of the flame across the particle surface is evident. The number of cycles can reach eight. This effect is due to the change of conversion stages. At air velocity above 95 m s^{-1} , fragmentation of fuel particles commences. A layer of char formed at an initial stage of burning heats up in the intensive air flow and is separated from the particle surface. The heated walls of the quartz channel contribute to the intensification of particle combustion. This effect is probably due to the swirling of the flame between the wall and the particle surface.



Citation: Svishchev, D. Experimental Study to Replicate Wood Fuel Conversion in a Downdraft Gasifier: Features and Mechanism of Single Particle Combustion in an Inert Channel. *Appl. Sci.* **2022**, *12*, 1179. <https://doi.org/10.3390/app12031179>

Academic Editor: Dmitrii O. Glushkov

Received: 15 November 2021

Accepted: 21 January 2022

Published: 23 January 2022

Publisher's Note: MDPI stays neutral with regard to jurisdictional claims in published maps and institutional affiliations.



Copyright: © 2022 by the author. Licensee MDPI, Basel, Switzerland. This article is an open access article distributed under the terms and conditions of the Creative Commons Attribution (CC BY) license (<https://creativecommons.org/licenses/by/4.0/>).

Keywords: biomass; downdraft gasification; single particle; combustion; mechanism; stages overlapping; fragmentation

1. Introduction

1.1. Background

Biomass is a renewable and promising energy source. It has a low cost, reduces countries dependence on fossil fuel supplies, and causes minimal environmental damage [1]. Compared to fossil fuels, the use of biomass yields lower carbon dioxide emissions [2–4]. Together with other renewable energy sources, biomass is seen as an element of sustainable development in a number of countries and regions [1,5]. Biomass has a number of features that complicate the feedstock supply chain and cause it to be used in plants of low unit capacity. Among these features are low calorific value and density of biomass, high moisture content, seasonal availability, and heterogeneity of geographical distribution [6].

There are three main approaches to energy conversion of biomass: thermochemical, biochemical, and physiochemical [7]. A promising method of thermochemical conversion is

the process of biomass gasification. In some cases, it proves more attractive than pyrolysis and combustion technologies from a technical and economic standpoint [8].

For small-scale power generation, biomass downdraft gasifier units are promising. Reactors of the downdraft type are characterized by simplicity of design and use, as well as small capital outlays. They make it possible to produce gas with low content of particles and tar [9]. Recent studies of biomass downdraft gasification are mainly aimed at solving the following problems:

1. Optimization of process parameters in order to reduce the yield of tar and char residue and increase cold gas efficiency and yield of target reaction products, such as hydrogen [10–12].
2. Significant reduction in the tar yield directly in the gasification process. This problem is solved by arranging additional reaction zones in the gasifier with the supply of the gasifying agent to these zones [13,14].
3. Effective cogasification of biomass with other fuels (coal, plastic, different types of waste, etc.), as well as cogasification of biomass of different origin [15–17].
4. Increasing the stability and automation of the gasification process [10,18,19].

A key defining feature of the process taking place in the downdraft gasifier is the high velocity of the gasifying agent relative to the fuel particles. Gas velocity at the tuyere outlet can reach 33 m s^{-1} [20]. In fluidized bed reactors, the agent velocity is $4\text{--}6 \text{ m s}^{-1}$ [21]. Gas velocity at entrained flow gasification is $15\text{--}30 \text{ m s}^{-1}$, but fuel particles $20\text{--}80 \mu\text{m}$ in size in these conditions move with the flow [22]. The tuyeres in the downdraft gasifier are located on the reactor surface. The high velocity allows the air jet to penetrate into the center of the fuel bed, which facilitates efficient oxidation and cracking of tar.

This paper is part of a larger study aimed at identifying the mechanism of wood downdraft gasification. The starting point of this study was the discovery of unconventional gasification conditions, as well as putting forward the hypothesis of an unstratified conversion mechanism [23]. The unconventional conditions were characterized by high cold gas efficiency, low reactor load sensitivity, compact reaction zone, etc. In further experimental works, it was established that there is no pyrolysis zone in some cases [24]. In other words, raw wood particles entered the area of the gasifier tuyeres and were gasified there. The process also had the properties mentioned above.

The paper deals with the combustion of single wood particles in an intense flow of tuyere air. To replicate the fuel bed, a wood particle was placed in a heated quartz channel. It is worth assuming that the bed particles significantly increase the intensity of each other's combustion due to an increase in the turbulent component of the heat and mass transfer processes. For example, in a study of combustion of graphite particles in a fluidized bed, there was a significant increase in the Sherwood number as the particle size of the inert material increased [25].

1.2. Combustion Mechanism of Single Fuel Particles

Studies on single-particle combustion are being carried out by a number of teams from Italy, Sweden, the UK, and other countries. The current interest in this research is due to the intensive development of oxy-fuel combustion technology, characterized by high environmental friendliness and the possibility of effective capture and storage of carbon dioxide. Studies of combustion of coke residue particles and coal in a fluidized bed [26–28], as well as biomass [29,30] are conducted.

The single particles combustion mechanism includes the stages of the release and combustion of volatiles (homogeneous process) and the combustion of a char residue (heterogeneous process). Depending on the combustion conditions these stages can proceed sequentially or overlap with each other.

Howard and Essenhigh found a significant overlapping between the homogenous and heterogeneous combustion stages of bituminous coal particles burning in pulverized fuel flames. With about 95% volatiles released from the fuel, about 50% of the coke residue was combusted at the same time [31]. Accounting for the fractional composition of fuel in the

mathematical model allowed the authors to establish a significant overlapping of stages for particles smaller than 15 microns, a slight overlapping for particles ranging from 15 to 65 microns, and staged combustion for particles larger than 65 microns. Tufano et al. later refined the Howard and Essenhigh data. Detailed kinetic modeling attests to the overlapping of volatile and coke residue combustion stages even for coal particles 100 microns in size [32].

Fuels with high volatile yields, such as biomass, are characterized by staged combustion, even for relatively small particles of 53–75 microns [33] and 0–100 microns [34]. However, spectral analysis of the radiation of burning biomass particles of 224–250 microns revealed a slight overlapping of the stages of homogeneous and heterogeneous combustion [35].

Large biomass particles burn mostly in separate stages. Remacha et al. found that the volatile matter flux from the particle surface is an order of magnitude greater than the flux of oxygen diffusing to the particle surface [36]. The volatile matter flux protects the solid surface of the particle from oxidation by oxygen. Mason et al. note the overlapping of stages of combustion, caused, however, by the asymmetry of particle heating, when the char residue begins to burn on one side of it, while the other is still completing the release of volatiles [37].

The subject of stages overlapping of solid fuels combustion remains poorly researched, which is evidenced by the almost complete absence of numerical metrics of this process. Only the work of D. Howard and R. Essenhigh, referred to above, notes a quantitative measure of overlap, but does not indicate how it was estimated [31]. Most papers provide a qualitative description of stage overlapping, following from visual observations or the results of mathematical modeling [38–40]. In this paper, we propose a technique for identifying the degree of overlapping of the char residue combustion stage with the devolatilization stage in the conversion of biomass particles.

2. Methods and Approaches

2.1. Single-Particle Combustion Method

For studying the combustion of particles in an intensive air flow we proposed and tested our own method [41]. Following this method, a sample is placed into the heated space of a furnace or channel and is blown over by air from a tuyere (Figure 1). The temperature of the air entering the tuyere is about room temperature (20–25 °C). The sample is held by a thermocouple with an open junction. The sample can be burned out completely or removed from the furnace after desired period of time measured from the moment the particle was placed in the furnace. Burning particles are quenched in the quenching chamber.

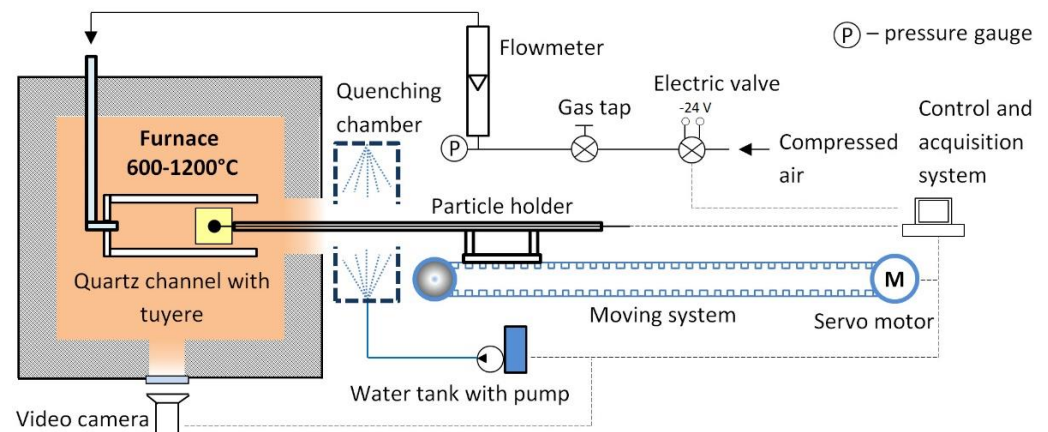


Figure 1. A schematic diagram of a rig for burning single fuel particles.

The reproducibility of the experiments is supported by automatic systems of the rig that are synchronized with each other (Figure 1). These systems are responsible for

air supply, sample movement and its quenching, temperature measurements, and video recording of the combustion process. Precise positioning of the sample in the furnace is ensured by a purpose-made sample holder with a precision movement mechanism.

Particles of similar initial sizes and weight, prepared from the same wood piece (pine) were used for tests. They were 12 ± 0.1 mm cubical shape particles weighing 671 ± 11 mg. Sample exposure in the furnace for different periods of time allows simulation of time-dependent change of mass, volume, and shape of a particle that is averaged over multiple samples.

After the experiment, samples were dried at 105 °C until they reached a constant weight. Part of the samples was used to determine the yield of volatiles and fixed carbon. The relative mass of charred particles (m , d.b.) was estimated as per the following expression:

$$m = \frac{m_{\text{sample}}}{m_0}, \quad (1)$$

where m_0 and m_{sample} —mass of the sample before and after the experiment. In addition, the mass of the char surface layer and the wood core, weakly affected by the thermochemical process, was determined. To perform the latter measurements, the surface char layer was peeled off from charred samples. The relative mass of the wood core (m_{core} , d.b.) and char layer (m_{char} , d.b.) was determined as per the Equations (2) and (3), respectively.

$$m_{\text{core}} = \frac{m_{\text{wood}}}{m_0} \quad (2)$$

$$m_{\text{char}} = \frac{m_{\text{char}}}{m_0} \quad (3)$$

2.2. Combustion Process Parameters

The air velocity in the tuyere of the rig varied from 10 to 125 m s⁻¹. The upper velocity value was chosen so as to be significantly higher than that in the downdraft gasifier. This choice allowed us to investigate atypical combustion conditions of the particles. The temperature in the experiments was 800 – 1200 °C, which corresponds to the level of temperatures achieved in the downdraft reactors [42–44].

In the first series of experiments, the particles were combusted in the furnace space, without a channel. Three heating temperatures were used: 800 , 1000 and 1200 °C. Different air flow rates were tested for each furnace temperature. Air flow velocity in the tuyere varied from 20 to 125 m s⁻¹.

In the second series of experiments a quartz channel was placed into the furnace that simulated the environment of bed particles (Figure 2). The channel was made of a quartz tube and was attached to the tuyere block. An inner diameter of a channel was 22 mm, and clearance between the particles' edge and an internal wall of the channel was 2.5 mm. The heating temperature during the experiments was 600 and 800 °C. Higher temperatures were not used because of the intense reaction of quartz and ash components at temperatures of 1000 °C and above. After several trials, the wall of the channel became opaque and its inner surface was covered with small pores. Air velocity in the tuyere varied from 10 to 125 m s⁻¹. In some experiments, the samples were burned out completely up to the moment of particle detachment from a holder by an air flow, or partially. In the latter case, the burning particles were removed and then quenched following the developed procedure.



Figure 2. Image of the quartz channel for particle combustion.

2.3. Types of Particle Holders

Two types of holders, which are different from each other in their design, were used. In the first type (type A), the air supply system is integrated with the thermocouple, on which the particle is mounted, and the tuyere and thermocouple move together with each other (Figure 3a). This type of holder is distinguished by the fact that in it the thermocouple wires are blown by a flow of cold tuyere air. The disadvantages of the first type of holder are the difficulty of using it together with the quartz channel, and the fact that the air flow tends to blow the particle off the thermocouple. The latter circumstance prevents the complete combustion of the samples.

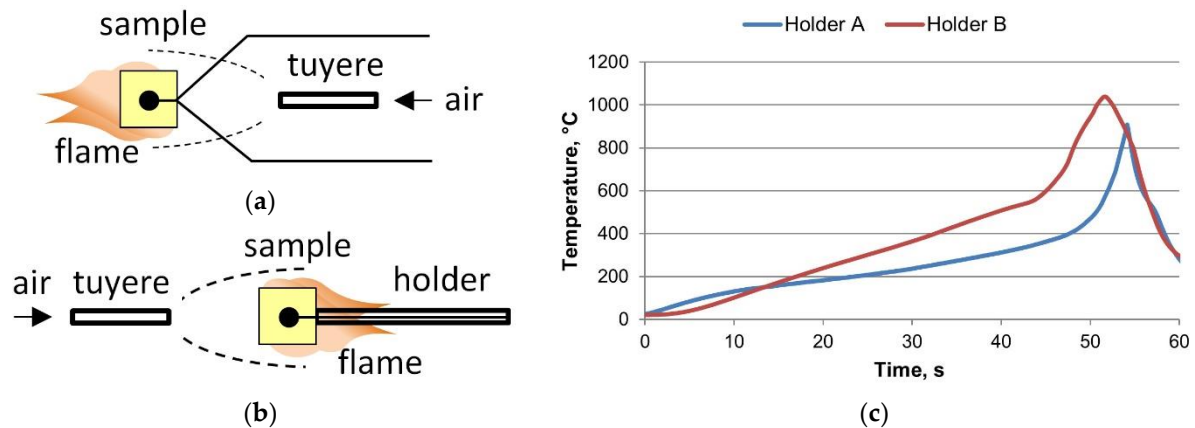


Figure 3. Types of particle holders (a,b) and their differences in recording temperature (c) given furnace temperature of 800 °C and air velocity of 20 m s⁻¹.

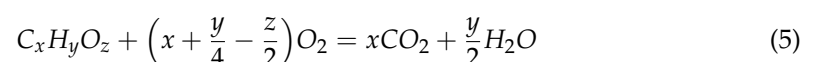
The second holder type (type B) moves the sample into and out of the furnace, while the tuyere and the inert channel are permanently installed in the furnace (Figure 3b). This holder type combines well with the inert channel but is characterized by heating of the thermocouple wires from the sample flame. The heat from the wires reaches the thermocouple junction, which distorts the measurement results. Protecting the wires with a ceramic sheath and steel cover only partially solves this problem.

Figure 3c shows the thermocouple junction temperature for different types of holders. The temperature profiles are similar to each other, but for the type B holder the heating is performed faster because it is affected by the flame from the sample. The type A holder is located outside the particle flame.

2.4. Process Metrics

The equivalence ratio was calculated as per Equation (4) as the weight ratio of the air supplied to the process to the air required for stoichiometrical combustion of fuel [45,46]. The latter magnitude was found as per Equation (5). The equivalence ratio can be estimated with a sufficient degree of accuracy only for the case of combustion of particles in the channel. The latter separates the sample space from the furnace space and allows the air in the furnace to be excluded from the heterogeneous combustion process.

$$ER = \frac{m_{\text{oxygen, supplied}}}{m_{\text{oxygen, stoichiometric}}} \quad (4)$$



Let us imagine that there is some idealized combustion process, which proceeds in separate stages. At the first stage of the process, the volatile matter is released from the sample and combusted, after the complete release of which the second stage of combustion

of the char residue begins. The condition of the absence of overlapping of the combustion stages of the particle by the time t can be represented by the following expression:

$$FC_c = FC_{pyro} - FC_t = 0, \quad (6)$$

where FC_c and FC_t burned and unburned parts of the char residue by the time t , respectively, FC_{pyro} —char residue obtained during pyrolysis of the particle. The fixed carbon of the fuel is not consumed during the devolatilization stage, and its amount in the charred sample remains constant and equal to the maximum amount.

When the combustion stages fully overlap, by the time t there is a quantitative consumption of the char layer formed on the surface of the particle:

$$FC_c = \max \quad (7)$$

Given complete combustion of the char layer, the residue of the particle will be raw wood, and the following ratio must be met:

$$\frac{FC_{pyro}}{VM_{pyro}} = \frac{FC_t}{VM_t} = \frac{FC_c}{VM_c}, \quad (8)$$

where VM is the volatile matter. From the expression (8) it follows that the maximum amount of burnt char residue will be:

$$FC_c = \frac{FC_{pyro} VM_c}{VM_{pyro}} \quad (9)$$

Based on the extreme conditions of overlapping of the stages (6) and (9), the degree of overlapping over time t can be found by the following equation:

$$X = \frac{FC_{pyro} - FC_t}{FC_{pyro} VM_c} VM_{pyro} = \frac{FC_{pyro} - FC_t}{FC_{pyro} - FC_{pyro} \frac{VM_t}{VM_{pyro}}} \quad (10)$$

In order to obtain charred samples, the entire particle combustion time range is divided into 10 intervals. At least two samples have to be obtained for each time interval, one of which is used to determine the mass of the wood core and surface layer of the char and the other one is required to determine the fixed carbon. To estimate the measurement uncertainty, one needs to test three to five parallel samples. The total number of samples, in this case, is 60–100 per one set of process parameters. When varying the parameters, the number of samples increases significantly, this makes conducting experiments much more time-consuming.

To reduce the number of experiments, the measurement uncertainty was estimated for one set of process parameters only. The assumption is made that changes in the process parameters do not significantly affect the uncertainty. The furnace temperature was assumed to be 800 °C, air velocity—20 m s⁻¹, the number of parallel samples—5 pcs. The samples were combusted in the furnace space. The standard deviation of the quantities of interest was as follows: m —2.9%, m_{core} —2.5%, m_{char} —0.7%, X —3.6%.

3. Results and Discussion

3.1. Furnace Space Particle Combustion

3.1.1. Particle Combustion Mechanisms

Combustion of single wood particles follows three possible mechanisms depending on the air flow velocity. The first mechanism is realized at an air flow velocity of 20 m s⁻¹ and lower. It is characterized by stage-wise nature. After the particle ignition, a flame of burning volatiles is formed around it (Figure 4a). This flame obstructs air penetration to the particle surface and prevents oxidation of a char layer. The front side of a particle remains cold and there is no flame near it.

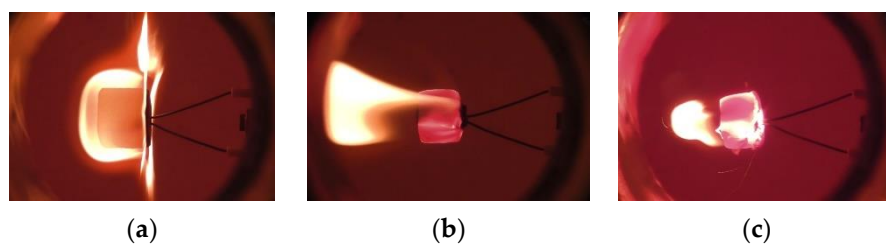


Figure 4. Stages of particle combustion at a furnace temperature of 800 °C and air flow velocity of 20 m s⁻¹, type A holder. Temperatures indicated under the figures are readings of the thermocouple in the center of a particle. (a) 138 °C, (b) 340 °C, (c) 820 °C.

Volatiles are released and burned at the first stage. A flame envelope is torn off from the particle surface when the temperature in its center is as high as 330–350 °C (Figure 4b). The flame base is located at the back face of a particle. After termination of the intensive release of volatiles the carbon residue of a particle starts to incandesce, and a stage of carbon residue combustion commences (Figure 4c).

A single-stage mechanism of particle combustion occurs at air velocity in the tuyere above 125 m s⁻¹. At the initial stage of particle combustion, its front edges and corners start incandescing, which evidences the burning of a char layer in those places (Figure 5a). A flame is not observed during burning. Incandescent areas gradually embrace the entire particle, but not its back face (Figure 5b). Particle center remains relatively cold. Its temperature is about 200 °C, which is not sufficient for the wood to be intensively decomposed. The center of a particle is heated to the temperature of pyrolysis commencement only when the burning front approaches it directly (Figure 5c). In a single-stage mechanism of combustion, the stages of volatile release and of char residue burning occur simultaneously.

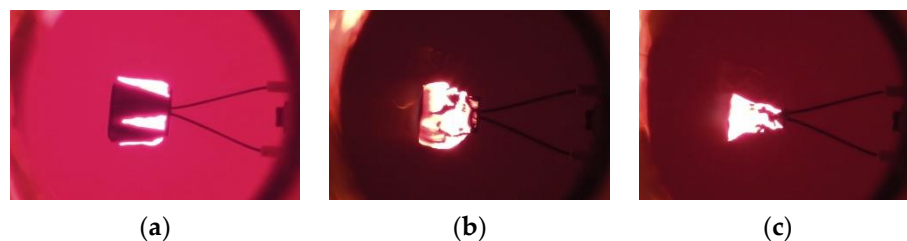


Figure 5. Particle combustion at a furnace temperature of 800 °C and air flow velocity of 125 ms⁻¹, type A holder. Figures below the pictures are temperatures at the center of a particle. (a) 173 °C, (b) 202 °C, (c) 285 °C.

With the velocity of air flow growing from 20 to 125 m s⁻¹, a two-stage conversion gradually changes over to a single-stage one. It is worthwhile mentioning that the temperature impact on the ranges in which some or other type of combustion mechanism occurs has not been observed. This impact is most probably irrelevant.

3.1.2. Particles Fragmentation during Combustion

Destruction of fuel particles into smaller ones is referred to as fragmentation. This phenomenon occurs in the process of fuel combustion, gasification and pyrolysis [47–49]. There are two types of fragmentation. Primary fragmentation is destruction of particles at stages of fuel drying and devolatilization [50–52]. It is due to mechanical stresses between different points of the same particle with different temperatures, and due to the destructive effect of the pressure of gas-vapor formed during pyrolysis. Secondary fragmentation occurs at a stage of char residues conversion and is conditioned by the growth of the porosity of the particles [53].

In a number of experiments, we observed the following mechanism of burning particle fragmentation. First, within several seconds after placing a sample into the furnace it

carbonizes (Figure 6a). Then the outer layer of char starts reacting with the air flow and rapidly incandesces (Figure 6b). The incandesced char layer is separated from the particle surface (Figure 6c). The major share of separated fragments remains fixed to the particle and burns near its surface, but some fragments are separated and fly to the furnace space. In Figure 6d, the separated fragment can be seen in the top right-hand part of the photo. Particle fragmentation is probably due to the following two causes. At rapid heating of the surface layer of char, intensive pyrolysis commences in the underlying layers of a particle. The gaseous products formed put pressure on the surface layer. During heating this layer expands, which facilitates its separation from the particle. The existence of a similar mixed mechanism of fragmentation was previously reported in the literature [50].

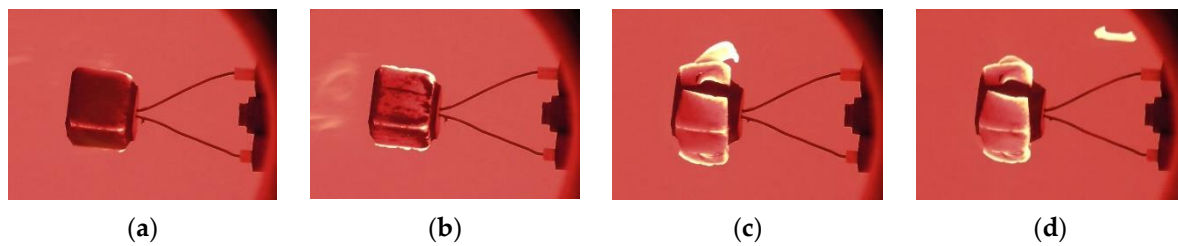


Figure 6. Particle fragmentation and preceding stages. Time elapsed after sample placing into the furnace is given under the photos. On the right of the photos a part of a type A holder is seen. (a) 4.3 s, (b) 4.5 s, (c) 5.0 s, (d) 5.4 s.

Fragmentation, to a certain extent, is a stochastic phenomenon, and the probability of its occurrence can conveniently be estimated by the fragmentation event rate [54]. This parameter is calculated as a ratio of fragmentation events to the total number of parallel samples tested under specified conditions. The number of parallel samples in the experiment ranged from three to five. From a statistical standpoint, this number is not large; therefore, estimation of fragmentation event rate was rather approximate.

Fragmentation event rate to a great extent depends on the velocity of the air coming to the particle from a tuyere, and to a lesser extent, on the furnace temperature (Table 1). At the air flow velocity of up to 50 m s^{-1} the fragmentation occurs rather rarely, and its event rate virtually vanishes. Starting from 60 m s^{-1} , the fragmentation event rate grows, and in the range of $95\text{--}125 \text{ m s}^{-1}$ it is observed in the major share of particles. Strong dependence of fragmentation event rate on the air velocity is consistent with the mechanism of process occurrence proposed above. Air flow reacts intensively with the char layer on the particle surface at high air velocity. Rapid heating of this layer accelerates particle pyrolysis and creates temperature stresses in the char layer.

Table 1. Fragmentation event rate (%) as a function of tuyere air velocity and furnace temperature.

T Furnace, °C	Air Flow, m s^{-1}					
	20	40	50	60	95	125
800	0	0	0	0	100	80
1000	0	0	0	50	100	100
1200	0	0	0	0	100	100

The fragmentation phenomenon is not desirable in the process of fuel combustion and gasification. It facilitates the formation of small char particles and their removal from the bed with ash, which reduces the efficiency of fuel conversion and aggravates the problems of solid residue utilization afterward [55].

3.1.3. Cyclic Movement of the Flame across the Particle Surface

Combustion of particles in the furnace space at air velocity of 20 m s^{-1} and furnace temperature of 800 °C is accompanied by an interesting effect. This effect consists in the

cyclic movement of the flame from the side face of the particle to its back face, and back to the side face (Figure 7).

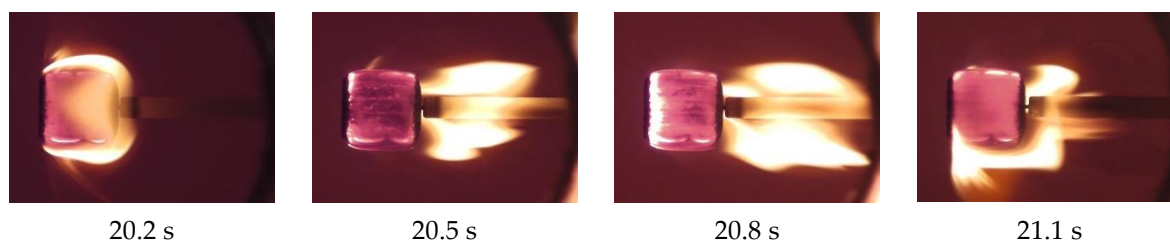


Figure 7. One of the cycles of changing the position of the flame during combustion of the particle (T furnace—800 °C, air velocity—20 m s⁻¹, type B holder without steel cover).

After the ignition of the particle, its surface is surrounded by flame, except for the front face. This facet faces the tuyere and is perpendicular to the axis of the air jet. The first movement of the flame is observed at 20.5 s from the start of the sample placement into the furnace. The air flow blows the flame off the side face, to which the flame returns after a certain time (21.1 s) and the cycle repeats again. The number of cycles varies from sample to sample and ranges from 6 to 8. The duration of the entire cyclic process takes about one third of the total combustion time of the particle (Table 2).

Table 2. Characteristics of the cyclic process.

Parameter	Magnitude
Total number of cycles	6–8
Cycle time, s	2.2–5.2
Total cyclic process time, s	18.5
The same, relative to the total combustion time of the particles, %	33
T center, °C:	
- at the beginning of the cyclic process	260
- at the end of the cyclic process	470

After the first movement of the flame, there is a decrease in the combustion rate of the particle. This can be seen from the change in the slope of the mass loss curve in the time interval from 18 to 24 s (Figure 8). It is worth assuming that such a decrease in the combustion rate is due to the movement of the flame away from the side face of the particle. The flame is the source of heat and charged particles needed to sustain the conversion process. In the absence of a flame, the char surface becomes exposed to oxidation by air, begins to react with it, and incandescens. Incandescing of the surface leads to heating up of the inner layers of the particle and intensification of their pyrolysis process with the release of volatiles to the surface. The mass loss rate of the particle increases again, and the volatile matter flame returns to side faces.

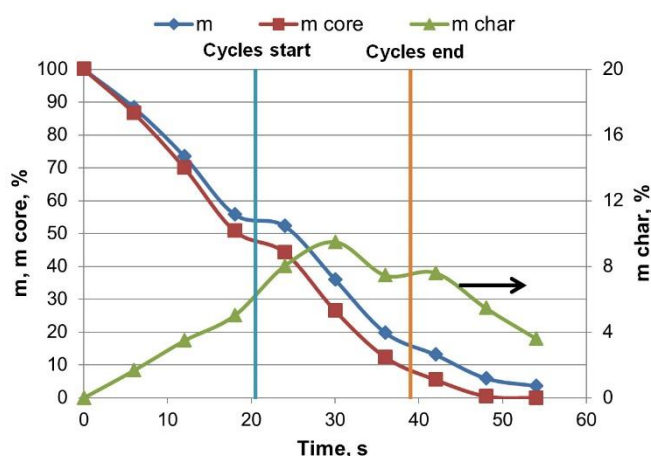


Figure 8. Change in the relative mass of the sample, its wood core and char layer over time (T furnace—800 °C, air velocity—20 m s⁻¹, burning takes place in the furnace space). The vertical lines indicate the beginning and end of the cyclic movement of the flame.

It should be noted that the middle of the time range of the cyclic process coincides with the maximum amount of char on the particle surface (Figure 8). It is likely that the cyclic movement of the flame is related to the change of combustion stages. The beginning of this process is due to the weakening of the sample devolatilization, and its end is marked by the completion of the devolatilization stage.

3.2. Particles Combustion in the Channel

3.2.1. Low Temperature Smoldering Combustion

Smoldering combustion is characteristic of particles in the channel at a furnace temperature of 600 °C. The combustion of the sample includes the charring and smoldering stages of the char layer of the particle. At low air velocities, smoldering that develops on the surface of the particle contributes to the ignition of volatiles. Further combustion of the particle occurs with the presence of flame on its side and back surface. When the air velocity is increased to 40–80 m s⁻¹, no flame is formed and the combustion of the sample proceeds completely as a smoldering process. The particle burns from the back to the side and front faces (Figure 9).

Significant amounts of smoke are emitted from samples in the absence of a flame. Tar particles that form smoke interact weakly with air oxygen due to low temperature and low concentration of radicals.

Changes in a number of particle parameters during smoldering combustion are shown in Figure 10. Particle conversion begins with a slow charring of its surface. It is only by the 27th second of the sample being in the furnace that the char on one of the particle vertices begins to smolder on the surface of the sample. In the time interval from 0 to 54 s, volatiles are released from the sample, and the consumption of the surface char layer proceeds relatively slowly. The degree of overlapping of the conversion stages (X) in this time interval proves close to zero, with predominantly heating and charring of the particles taking place. In the time interval between 40 and 60 s, negative values of X are observed. Such values are due to the fact that the yield of fixed carbon from the charred samples exceeds the yield of carbon from raw wood. A similar phenomenon was noted earlier in J.J. Saastamoinen et al. and explained by chemisorption of oxygen on the carbon surface [56].

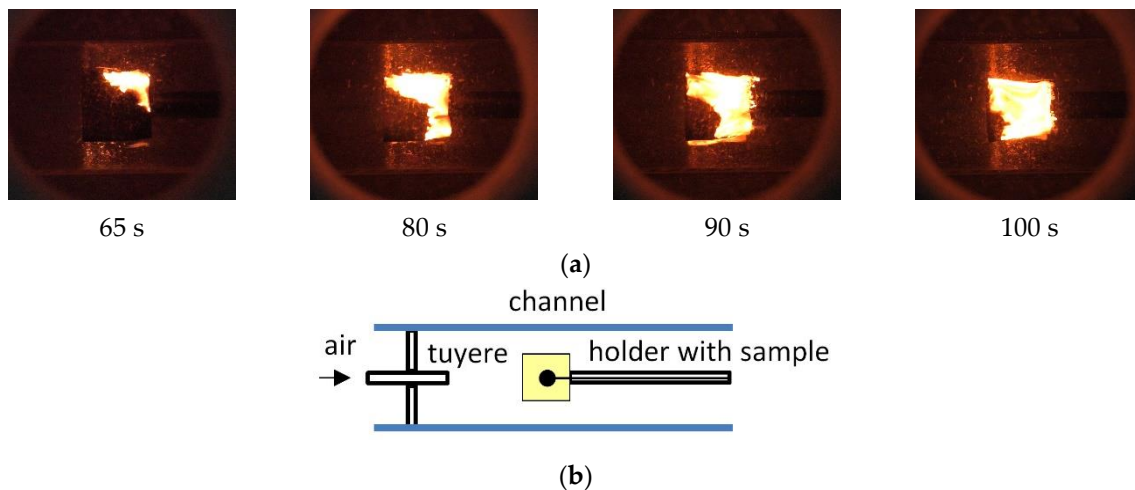


Figure 9. Flameless combustion of the sample in an inert channel, $T_{\text{furnace}}=600\text{ }^{\circ}\text{C}$, air velocity— 40 m s^{-1} , type B holder with a steel cover (a). The following images show the time starting from the moment the sample is put into the furnace. Diagram (b) explains the location of the particle and the elements of the rig.

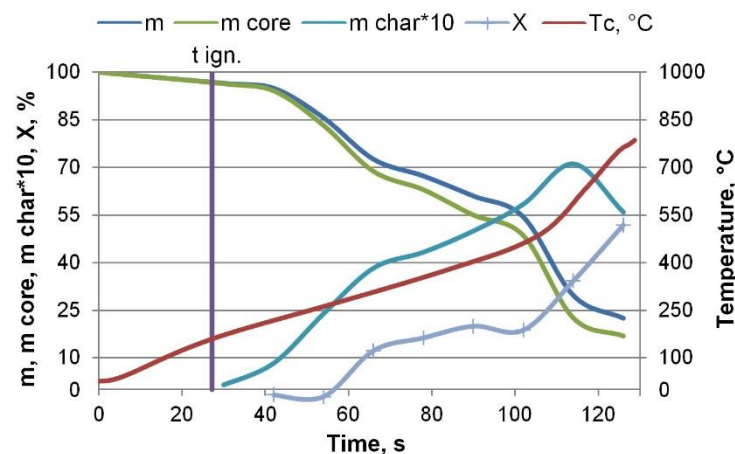


Figure 10. Changing of parameters of particle smoldering process ($T_{\text{furnace}}=600\text{ }^{\circ}\text{C}$, air velocity— 40 m s^{-1} , combustion in the channel): m —relative mass of the charred particle, m_{core} —mass of particle wood core, m_{char} —mass of char layer, X —degree of overlapping of stages; t_{ign} —average time of particle smoldering start, s; T_c —temperature of sample center, $^{\circ}\text{C}$.

In the time interval from 54 to 102 s, the process of smoldering of the char layer, which spreads over the surface of the particle, evolves. Smoldering results in char consumption. The overlapping of the char residue combustion stage with the devolatilization stage is 12–19% in this case. The growth rate of the surface char layer mass slows down. By the 102nd second of the process, the thermocouple readings reach $460\text{ }^{\circ}\text{C}$. This level of temperature is sufficient to complete the intensive release of volatiles from the particle. Nevertheless, by the 102nd second of conversion, the wood core remains in the sample, with a weight of 49% of the initial particle weight. Under the experimental conditions, heat comes to the thermocouple junction from the holder heated in the furnace, despite the protective outer steel cover and the ceramic protection sheath that thermocouple wires run through.

After 103–104 s of sample combustion, the char layer smoldering process spreads to all side and back faces of the particle, which further leads to a simultaneous increase in the rate of consumption and formation of the char layer. The mass of this layer peaks at 7% by the 114th second of sample combustion. It is noteworthy that at the maximum yield

of char, the wood part remains in the sample, the mass of which is 23% of the initial mass of the sample. The unconverted wood residue is located in the frontal part of the sample, which is hit by a flow of the cold tuyere air.

3.2.2. Two-Stage Particle Combustion Mechanism

Combustion at an air velocity of 20 m s^{-1} and a furnace temperature of $800 \text{ }^\circ\text{C}$ is characterized by the presence of a flame of volatile matter near the side and back faces of the particle. The time delay between placing the sample into the furnace and its ignition is significantly shorter than in the case of a similar air velocity and a furnace temperature of $600 \text{ }^\circ\text{C}$. This delay is 3 s compared to 55 s, respectively. During the first 6 s of conversion, the particle intensely loses volatile substances and gets charred (Figure 11). In this case, the surface char layer is virtually not consumed, and the degree of overlapping of the stages is 4%.

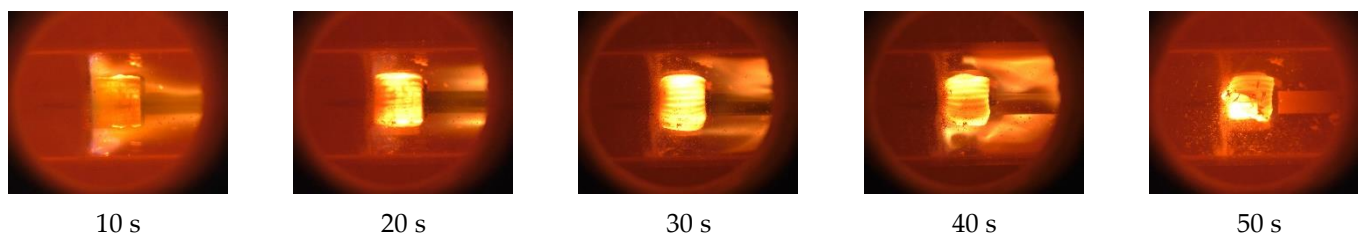
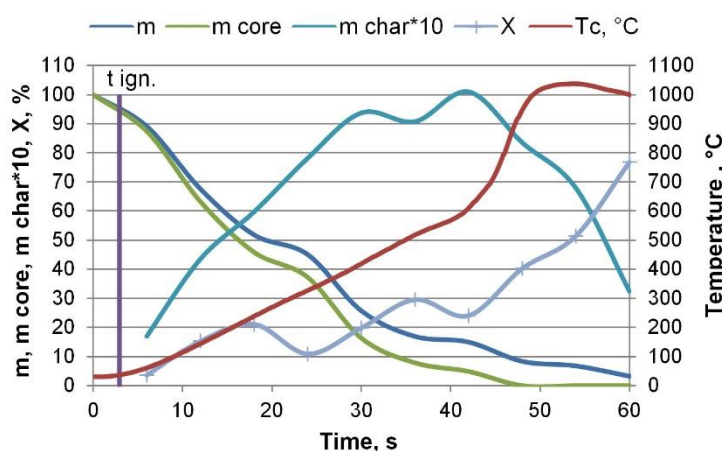


Figure 11. Characteristics of two-stage combustion of wood particles in the channel at T_{furnace} of $800 \text{ }^\circ\text{C}$ and air velocity of 20 m s^{-1} : m —mass of the charred particle, m_{core} —mass of particle wood core, m_{char} —mass of the char layer, X —degree of overlapping of stages; $t_{\text{ign.}}$ —average time of particle ignition start, s; T_c —temperature of sample center, $^\circ\text{C}$.

From the sixth second of particle combustion on, simultaneously with devolatilization and an increase in the mass of the surface char layer, the char layer also gets consumed. The relative content of fixed carbon (FC/FC_{pyro}) in the charred sample decreases from 98% to 78% from the sixth to the 42nd second. In this time interval, the degree of stage overlapping ranges from 12 to 24%.

The maximum amount of char is formed in the particle at the 42nd second of conversion and is 10% of the sample initial mass. The degree of stage overlapping by this point is 24%. It should be noted that simultaneously with the maximum mass of char, the charred sample contains a wood residue with a relative mass of 5%. By the 48th second of the process, the sample is already completely composed of the char and the combustion stage of the char residue becomes the main one.

The temperature of the thermocouple junction increases almost linearly from the sixth to the 42nd second of the process. Thermocouple readings are significantly affected by the flame of volatiles surrounding the sample holder and heating the thermocouple wires.

Nevertheless, the course of the temperature profile reflects the change from the stage when devolatilization prevails to the stage when combustion of the char residue prevails. From the 42nd second on, the heating rate of the thermocouple junction increases significantly.

Combustion of samples at a furnace temperature of 800 °C and air velocity of 20 m s⁻¹ can be characterized as a predominantly staged process, with the degree of overlapping of the char residue combustion stage with the devolatilization stage of 6 to 40%, depending on the considered time interval of sample combustion.

3.2.3. Single-Stage Particle Combustion Mechanism

The process of particle combustion at a furnace temperature of 800 °C and air velocity of 125 m s⁻¹, has common features with the aforementioned smoldering combustion. From the moment the sample is put into the furnace until the fifth second, the sample is heated and charred. Then the individual dots on the side and back faces of the particle begin to smolder and glow. By the 22nd second, the glow area spreads along the entire length of the faces, and by the 43rd second, it covers all the side and back faces. The change in the relative mass loss of the sample (m) is consistent with the propagation of the glow region; the conversion process accelerates with the increase in the smoldering surface of the particle (Figure 12).

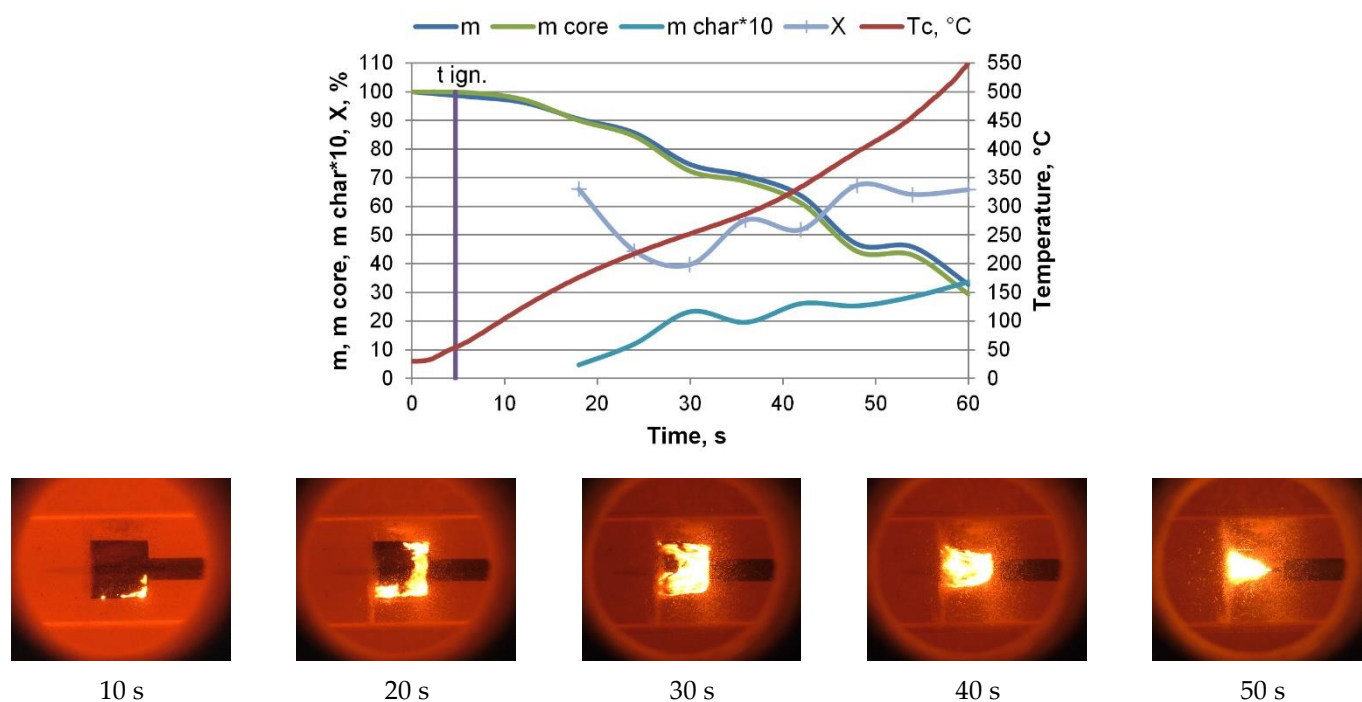


Figure 12. Characteristics of single-stage combustion of wood particles, $T_{furnace}$ —800 °C, air velocity—125 m s⁻¹: m —mass of the charred particle, m_{core} —mass of particle wood core, m_{char} —mass of the char layer, X —degree of overlapping of stages; $t_{ign.}$ —average time of particle ignition start, s; T_c —temperature of the sample center, °C.

Charred wood fuel samples tested under these conditions and taken out of the furnace at different times consist almost entirely of an unreacted wood core surrounded by a thin layer of char (Figure 12). Combustion is characterized by a small degree of char accumulation on the particle surface and a significant overlapping of the char residue combustion stage with the devolatilization stage. The degree of overlapping of the process stages at a furnace temperature of 800 °C and air velocity of 125 m s⁻¹ ranges from 40 to 68%.

The degree of overlapping of combustion stages can be estimated not only for the overall process running from the beginning of sample input to the time t , but also for

different time intervals. For example, the initial period of sample conversion time can be excluded from the calculation of X . During this period, the charring of the particle occurs, and the smoldering of the charcoal layer begins and evolves. The initial period is transitional and does not fully characterize the course of the main combustion process. If it is excluded, the degree of stage overlapping increases at various time intervals up to 60–95% (Figure 13). A significant overlapping of the conversion stages allows us to characterize this kind of sample combustion process as predominantly single-stage, in which the consumption of most of the char occurs simultaneously with the process of heating and wood pyrolysis.

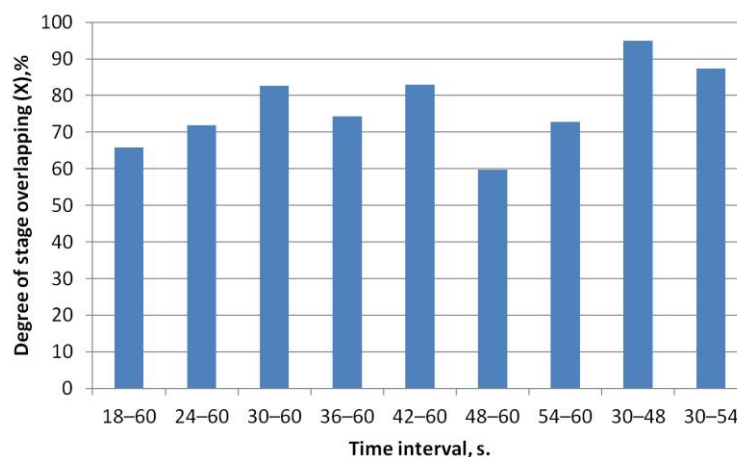


Figure 13. Degree of overlapping of the devolatilization and char residue combustion stages in a single-stage conversion process. The time intervals used to evaluate the degree of overlapping are indicated.

In the investigated single-stage process, the flame on the surface of the particle and in the inert channel behind it is visually absent, and smoke, which is gas sol from the tar particles, comes out of the exhaust port of the rig. The cumulative particle conversion process is characterized by a high equivalence ratio of 6.3. The air flow rate far exceeds the needs of the combustion process in the oxidizer. The products of combustion are greatly diluted with cold air, and the intense flow of the latter quickly carries the products out of the furnace. The low temperature and relatively short residence time of the vapor-gas conversion products in the furnace result in a high tar content in the exhaust.

The equipment that consumes producer gas can have high standards with respect to gas quality. Depending on the technology of gas use, the amount of tar in it should not exceed the level of 0.1–100 mg/m³ [57–59]. Fuel gasification conditions with insufficient tar conversion can also take place in downdraft gasifiers operating with intensive air supply to the reactor. The capacity of gasifiers of this type is limited by the 1.4–2.5 MW range with respect to fuel and is associated with the unsatisfactory quality of the gasifier gas obtained by scaling up and boosting the reactor of the unit [60–62].

3.3. Comparison of Particle Combustion in the Channel and Furnace Space

Figure 14 shows the change in readings of the thermocouple installed at the center of the particles. Most temperature profiles are characterized by the maximum value due to the intense heating of the thermocouple junction when char or wood residue burns near it. The temperature maximum corresponds to the moment of detachment from the holder or afterburning of the particle residue on it and can be used to estimate the complete combustion time of the samples.

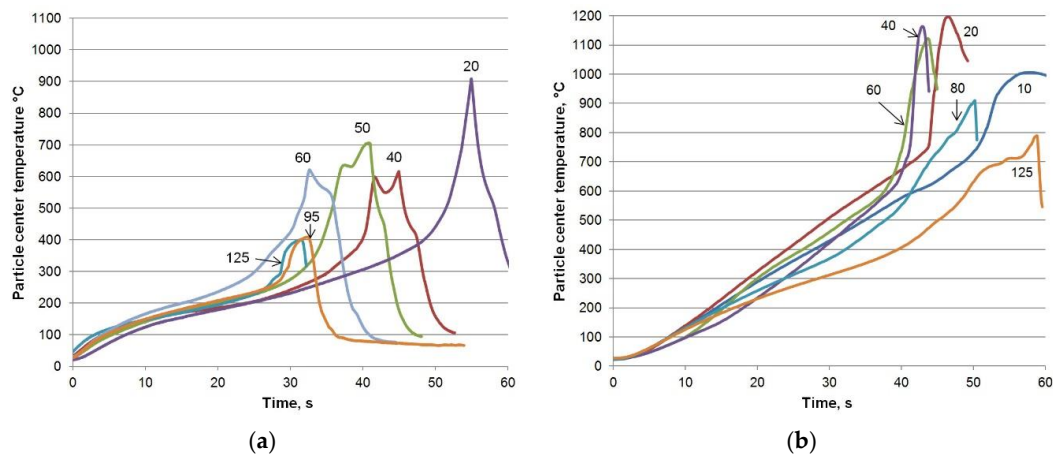


Figure 14. Change of particle center temperature in time at different tuyere air velocity. Combustion in the free space of the furnace (a) and the inert channel (b), $T_{\text{furnace}}=800\text{ }^{\circ}\text{C}$, the captions indicate air velocities.

When testing the particles in the free space of the furnace, increasing the air velocity leads to a decrease in their combustion time (Figure 14a).

The experiments with the inert channel are characterized by a slightly different pattern. An initial increase in air velocity from 10 m s^{-1} to 40 m s^{-1} leads to an intensification of the process and a decrease in the combustion time of the particles (Figure 14b). A further increase in air velocity causes the opposite effect, which is an increase in combustion time. Differences between the dynamics of combustion of particles in the furnace and the channel can be explained by the different temperatures of the air supplied to the surface of the samples. In the first case, the tuyere flow was mixed with the heated air in the muffle. In the second case, channel design excluded hot air injection from the furnace space, and cold tuyere air was supplied to the sample. Thermocouple measurements showed that the difference in air temperature between the first and the second case was $150\text{--}200\text{ }^{\circ}\text{C}$.

It is interesting to compare the cases of combustion of particles in the furnace and the channel as performed at 20 m s^{-1} and $800\text{ }^{\circ}\text{C}$. Measurements indicate the different temperatures of the air supplied to the particles under these conditions. In spite of this, the experiments produce the dynamics of the particle mass change that are similar to each other (Figure 15). It is likely that this pattern is due to the presence of a flame swirl between the particle and the channel, which contributes heat to the combustion process and compensates for the lower air temperature. The pattern confirms the hypothesis, as put forward by the study, of the intensification of the process of combustion of particles in the inert channel.

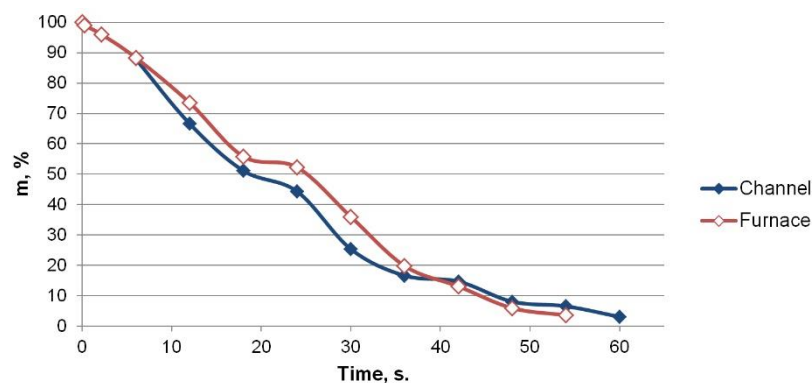


Figure 15. The change in particle mass over time at a furnace temperature of $800\text{ }^{\circ}\text{C}$ and air flow velocity of 20 m s^{-1} .

4. Conclusions

As part of the work, visual observation of combustion and measurement of the temperature of the center of the particles were carried out. The particles were burned in the furnace space, and the furnace temperature and air velocity were varied in the experiments. This study showed the existence of two mechanisms of particle combustion, namely two-stage and single-stage. In the range of tuyere air velocity below 20 m s^{-1} , the two-stage process occurs. Volatiles are released from the particle and burn at the initial stage of this process. Flame around the particle, with the help of the flow of conversion products, limits the diffusion of oxygen to the char surface of the particles and also chemically binds it during the oxidation of combustible components. Char residue burns at the second stage of the process. At the air velocity above 125 m s^{-1} a single-stage mechanism of single particles combustion prevails. Intensive air flow reaches the fuel particle surface and causes burning of a surface layer of char. The stages of devolatilization of fuel and that of char residue combustion occur simultaneously. In single-stage combustion, there is no flame around the particles.

At the tuyere air velocity above $60\text{--}95 \text{ m s}^{-1}$ the fragmentation of fuel particles commences. The surface layer of char formed on the particle surface starts intensively reacting with the air oxygen, which may cause its rapid heating and separation from the particle.

In this study, combustion conditions were found under which cyclic movement of the flame across the surface of the particle is observed. This process takes about one third of the total combustion time of the particle and consists of 6–8 cycles. Cyclicity might be due to the changing stages of combustion of volatiles and char residue. If there is a flame near the surface of the particle, the release of volatiles slows down over time. This deceleration leads to a flame blowout and intense subsequent combustion of the char layer. This layer heats the particle's wood core and intensifies the pyrolytic processes in it. An increase in the release of volatiles in turn contributes to the return of the flame to the surface of the particle. The cyclic process takes place during the period of change of the devolatilization to the char residue combustion stage.

The combustion of particles in the channel at low temperature ($600 \text{ }^\circ\text{C}$) proceeds with a prolonged charring stage of the sample and the subsequent spread of smoldering over the char layer. At air velocities up to $40\text{--}80 \text{ m s}^{-1}$, flame formation around the sample is observed. At high air velocities, there is no flame, and the process proceeds with the formation of large amounts of smoke, the particles of which consist mainly of tar.

The degree of overlapping of stages proposed in the study provides a quantitative assessment of the combustion conditions and allows us to determine the mechanism of the process. The two-stage process of particle combustion in the channel is characterized by a relatively small degree of stage overlap, amounting to 24%. The observed process is far from the ideal case in which there is complete separation of the stages, and it can be characterized as predominantly two-stage. By contrast, the single-stage process is characterized by a stage overlapping degree of 60–95% for different combustion time intervals. This process is also far from ideal and can be characterized as predominantly single-stage since there is always a small layer of burning char on the surface of the particle.

The heated walls of the channel intensify the process of particle combustion. Such an effect is probably due to the swirling of the flame between the particle and the channel.

Funding: The research was carried out under State Assignment Project (no. FWEU-2021-0005) of the Fundamental Research Program of Russian Federation 2021-2030: FWEU-2021-0005; partly supported by the Russian Foundation of Basic Research, No 18-29-24047 using the resources of the High-Temperature Circuit Multi-Access Research Center (Ministry of Science and Higher Education of the Russian Federation, project no 13.CKP.21.0038): 18-29-24047.

Institutional Review Board Statement: Not applicable.

Informed Consent Statement: Not applicable.

Data Availability Statement: Not applicable.

Conflicts of Interest: The author declares no conflict of interest.

References

1. Güney, T.; Kantar, K. Biomass energy consumption and sustainable development. *Int. J. Sustain. Dev. World Ecol.* **2020**, *27*, 762–767. [[CrossRef](#)]
2. Solarin, S.A.; Al-Mulali, U.; Gan, G.G.G.; Shahbaz, M. The impact of biomass energy consumption on pollution: Evidence from 80 developed and developing countries. *Environ. Sci. Pollut. Res.* **2018**, *25*, 22641–22657. [[CrossRef](#)] [[PubMed](#)]
3. Sayed, E.T.; Wilberforce, T.; Elsaid, K.; Rabaia, M.K.H.; Abdelkareem, M.A.; Chae, K.-J.; Olabi, A.G. A critical review on environmental impacts of renewable energy systems and mitigation strategies: Wind, hydro, biomass and geothermal. *Sci. Total Environ.* **2021**, *766*, 144505. [[CrossRef](#)] [[PubMed](#)]
4. Danish; Wang, Z. Does biomass energy consumption help to control environmental pollution? Evidence from BRICS countries. *Sci. Total Environ.* **2019**, *670*, 1075–1083. [[CrossRef](#)] [[PubMed](#)]
5. Ajmi, A.N.; Inglesi-Lotz, R. Biomass energy consumption and economic growth nexus in OECD countries: A panel analysis. *Renew. Energy* **2020**, *162*, 1649–1654. [[CrossRef](#)]
6. Nunes, L.J.R.; Causer, T.P.; Ciolkosz, D. Biomass for energy: A review on supply chain management models. *Renew. Sustain. Energy Rev.* **2020**, *120*, 109658. [[CrossRef](#)]
7. Adams, P.; Bridgwater, T.; Lea-Langton, A.; Ross, A.; Watson, I. Biomass Conversion Technologies. In *Greenhouse Gas Balances of Bioenergy Systems*; Elsevier: Amsterdam, The Netherlands, 2018; pp. 107–139. ISBN 978-0-08-101036-5.
8. Solarte-Toro, J.C.; González-Aguirre, J.A.; Giraldo, J.A.P.; Alzate, C.A.C. Thermochemical processing of woody biomass: A review focused on energy-driven applications and catalytic upgrading. *Renew. Sustain. Energy Rev.* **2021**, *136*, 110376. [[CrossRef](#)]
9. Situmorang, Y.A.; Zhao, Z.; Yoshida, A.; Abudula, A.; Guan, G. Small-scale biomass gasification systems for power generation (<200 kW class): A review. *Renew. Sustain. Energy Rev.* **2019**, *117*, 109486. [[CrossRef](#)]
10. Susastriawan, A.A.P.; Saptoadi, H. Purnomo Small-scale downdraft gasifiers for biomass gasification: A review. *Renew. Sustain. Energy Rev.* **2017**, *76*, 989–1003. [[CrossRef](#)]
11. Ngamsidhipongsas, N.; Ponpesh, P.; Shotipruk, A.; Arpornwichanop, A. Analysis of the Imbert downdraft gasifier using a species-transport CFD model including tar-cracking reactions. *Energy Convers. Manag.* **2020**, *213*, 112808. [[CrossRef](#)]
12. Prasertcharoensuk, P.; Hernandez, D.A.; Bull, S.J.; Phan, A.N. Optimisation of a throat downdraft gasifier for hydrogen production. *Biomass Bioenergy* **2018**, *116*, 216–226. [[CrossRef](#)]
13. Zhao, X.; Li, K.; Lamm, M.E.; Celik, S.; Wei, L.; Ozcan, S. Solid Waste Gasification: Comparison of Single- and Multi-Staged Reactors. In *Gasification*; IntechOpen: London, UK, 2021.
14. Saleh, A.R.; Sudarmanta, B.; Fansuri, H.; Muraza, O. Improved Municipal Solid Waste Gasification Efficiency Using a Modified Downdraft Gasifier with Variations of Air Input and Preheated Air Temperature. *Energy Fuels* **2019**, *33*, 11049–11056. [[CrossRef](#)]
15. Thengane, S.K.; Gupta, A.; Mahajani, S.M. Co-gasification of high ash biomass and high ash coal in downdraft gasifier. *Bioresour. Technol.* **2019**, *273*, 159–168. [[CrossRef](#)] [[PubMed](#)]
16. Donskoy, I. Mathematical modelling and optimization of biomass-plastic fixed-bed downdraft co-gasification process. *EPJ Web Conf.* **2017**, *159*, 00010. [[CrossRef](#)]
17. Awais, M.; Omar, M.M.; Munir, A.; Li, W.; Ajmal, M.; Hussain, S.; Ahmad, S.A.; Ali, A. Co-gasification of different biomass feedstock in a pilot-scale (24 kWe) downdraft gasifier: An experimental approach. *Energy* **2022**, *238*, 121821. [[CrossRef](#)]
18. Zachl, A.; Buchmayr, M.; Gruber, J.; Anca-Couce, A.; Scharler, R.; Hochenauer, C. Evaluation and extension of the load and fuel flexibility limits of a stratified downdraft gasifier. *Energy* **2022**, *239*, 122279. [[CrossRef](#)]
19. Zachl, A.; Buchmayr, M.; Gruber, J.; Anca-Couce, A.; Scharler, R.; Hochenauer, C. Shifting of the flame front in a small-scale commercial downdraft gasifier by water injection and exhaust gas recirculation. *Fuel* **2021**, *303*, 121297. [[CrossRef](#)]
20. Reed, T.B.; Das, A. *Handbook of Biomass Downdraft Gasifier Engine Systems*; Biomass Energy Foundation Press: Franktown, CO, USA, 1998; ISBN 978-1-60322-040-8.
21. Basu, P. *Combustion and Gasification in Fluidized Beds*; CRC Press: Boca Raton, FL, USA, 2006; ISBN 0-8493-3396-2.
22. Gräbner, M. *Industrial Coal Gasification Technologies Covering Baseline and High-Ash Coal*; Wiley: Hoboken, NJ, USA, 2014; ISBN 978-3-527-33693-7.
23. Svishchev, D.A.; Kozlov, A.N.; Donskoy, I.G.; Ryzhkov, A.F. A semi-empirical approach to the thermodynamic analysis of downdraft gasification. *Fuel* **2016**, *168*, 91–106. [[CrossRef](#)]
24. Svishchev, D.A.; Kozlov, A.N.; Penzik, M.V. Unstratified Downdraft Gasification: Conditions for Pyrolysis Zone Existence. *Energy Procedia* **2019**, *158*, 649–654. [[CrossRef](#)]
25. Hayhurst, A.N.; Parmar, M.S. Measurement of the mass transfer coefficient and Sherwood number for carbon spheres burning in a bubbling fluidized bed. *Combust. Flame* **2002**, *130*, 361–375. [[CrossRef](#)]
26. Roy, B.; Bhattacharya, S. Combustion of single char particles from Victorian brown coal under oxy-fuel fluidized bed conditions. *Fuel* **2016**, *165*, 477–483. [[CrossRef](#)]
27. Chao, J.; Yang, H.; Wu, Y.; Zhang, H.; Lv, J.; Dong, W.; Xiao, N.; Zhang, K.; Xu, C. The investigation of the coal ignition temperature and ignition characteristics in an oxygen-enriched FBR. *Fuel* **2016**, *183*, 351–358. [[CrossRef](#)]

28. Scala, F. Fluidized-Bed Combustion of Single Coal Char Particles: An Analysis of the Burning Rate and of the Primary CO/CO₂ Ratio. *Energy Fuels* **2011**, *25*, 1051–1059. [[CrossRef](#)]
29. Bu, C.; Leckner, B.; Chen, X.; Pallarès, D.; Liu, D.; Gómez-Barea, A. Devolatilization of a single fuel particle in a fluidized bed under oxy-combustion conditions. Part A: Experimental results. *Combust. Flame* **2015**, *162*, 797–808. [[CrossRef](#)]
30. Riaza, J.; Khatami, R.; Levendis, Y.A.; Álvarez, L.; Gil, M.V.; Pevida, C.; Rubiera, F.; Pis, J.J. Combustion of single biomass particles in air and in oxy-fuel conditions. *Biomass Bioenergy* **2014**, *64*, 162–174. [[CrossRef](#)]
31. Howard, J.B.; Essenhigh, R.H. Mechanism of solid-partial combustion with simultaneous gas-phase volatiles combustion. *Symp. Combust.* **1967**, *11*, 399–408. [[CrossRef](#)]
32. Tufano, G.L.; Stein, O.T.; Kronenburg, A.; Gentile, G.; Stagni, A.; Frassoldati, A.; Faravelli, T.; Kempf, A.M.; Vascellari, M.; Hasse, C. Fully-resolved simulations of coal particle combustion using a detailed multi-step approach for heterogeneous kinetics. *Fuel* **2019**, *240*, 75–83. [[CrossRef](#)]
33. Zhang, Y.; Zhao, J.; Ma, Z.; Yang, F.; Cheng, F. Effect of oxygen concentration on oxy-fuel combustion characteristic and interactions of coal gangue and pine sawdust. *Waste Manag.* **2019**, *87*, 288–294. [[CrossRef](#)]
34. Ye, B.; Zhang, R.; Cao, J.; Lei, K.; Liu, D. The study of co-combustion characteristics of coal and microalgae by single particle combustion and TGA methods. *J. Energy Inst.* **2020**, *93*, 508–517. [[CrossRef](#)]
35. Weng, W.; Costa, M.; Aldén, M.; Li, Z. Single particle ignition and combustion of pulverized pine wood, wheat straw, rice husk and grape pomace. *Proc. Combust. Inst.* **2019**, *37*, 2663–2671. [[CrossRef](#)]
36. Remacha, M.P.; Jiménez, S.; Ballester, J. Devolatilization of millimeter-sized biomass particles at high temperatures and heating rates. Part 2: Modeling and validation for thermally-thin and -thick regimes. *Fuel* **2018**, *234*, 707–722. [[CrossRef](#)]
37. Mason, P.E.; Darvell, L.I.; Jones, J.M.; Pourkashanian, M.; Williams, A. Single particle flame-combustion studies on solid biomass fuels. *Fuel* **2015**, *151*, 21–30. [[CrossRef](#)]
38. Shan, F.; Lin, Q.; Zhou, K.; Wu, Y.; Fu, W.; Zhang, P.; Song, L.; Shao, C.; Yi, B. An experimental study of ignition and combustion of single biomass pellets in air and oxy-fuel. *Fuel* **2017**, *188*, 277–284. [[CrossRef](#)]
39. Mock, C.; Lee, H.; Choi, S.-C.; Yang, W.; Choi, S.; Manovic, V. Combustion Behavior of Single Pellets of Coal–Wood Mixtures in a Hot Gas Flow Field. *Energy Fuels* **2018**, *32*, 11913–11923. [[CrossRef](#)]
40. Veras, C.A.G.; Saastamoinen, J.; Carvalho, J.A., Jr.; Aho, M. Overlapping of the Devolatilization and Char Combustion Stages in the Burning of Coal Particles. *Combust. Flame* **1999**, *116*, 567–579. [[CrossRef](#)]
41. Svishchev, D.A.; Kozlova, M.A.; Ralnikov, P.A. A Method of Studying Thermochemical Conversion of Single Biomass Particles in an Intense Air Flow. *J. Phys. Conf. Ser.* **2019**, *1261*, 012036. [[CrossRef](#)]
42. Rabea, K.; Bakry, A.I.; Khalil, A.; El-Fakharany, M.K.; Kadous, M. Real-Time Performance Investigation of a Downdraft Gasifier Fueled by Cotton Stalks in a Batch-Mode Operation. *Fuel* **2021**, *300*, 120976. [[CrossRef](#)]
43. Pandey, B.; Prajapati, Y.K.; Sheth, P.N. CFD analysis of biomass gasification using downdraft gasifier. *Mater. Today Proc.* **2021**, *44*, 4107–4111. [[CrossRef](#)]
44. Elshokary, S.; Farag, S.; Sayed Mohamed Abu-Elyazeed, O.; Hurisso, B.; Ismai, M. Downdraft Gasifier Design Calculation for Biomass Gasification Using Exhaust Gas as a Gasification Agent. *Mater. Today Proc.* **2021**, S2214785321026055. [[CrossRef](#)]
45. Gálvez-Pérez, A.; Martín-Lara, M.A.; Calero, M.; Pérez, A.; Canu, P.; Blázquez, G. Ex-perimental Investigation on the Air Gasification of Olive Cake at Low Temperatures. *Fuel Process. Technol.* **2021**, *213*, 106703. [[CrossRef](#)]
46. Choi, M.-J.; Jeong, Y.-S.; Kim, J.-S. Air gasification of polyethylene terephthalate using a two-stage gasifier with active carbon for the production of H₂ and CO. *Energy* **2021**, *223*, 120122. [[CrossRef](#)]
47. Kuznetsov, G.V.; Syrodoy, S.V.; Gutareva, N.Y.; Kostoreva, A.A.; Kostoreva, Z.A. Ignition of the wood biomass particles under conditions of near-surface fragmentation of the fuel layer. *Fuel* **2019**, *252*, 19–36. [[CrossRef](#)]
48. Caposciutti, G.; Almuina-Villar, H.; Dieguez-Alonso, A.; Gruber, T.; Kelz, J.; Desideri, U.; Hochenauer, C.; Scharler, R.; Anca-Couce, A. Experimental investigation on biomass shrinking and swelling behaviour: Particles pyrolysis and wood logs combustion. *Biomass Bioenergy* **2019**, *123*, 1–13. [[CrossRef](#)]
49. Cui, T.; Xu, J.; Fan, W.; Chang, Q.; Yu, G.; Wang, F. Experimental study on fragmental behavior of coals and biomasses during rapid pyrolysis. *Bioresour. Technol.* **2016**, *222*, 439–447. [[CrossRef](#)] [[PubMed](#)]
50. Litun, D.S.; Ryabov, G.A. Modern State and Topical Issues of Studying Solid Fuel Particle Primary Fragmentation Processes as Applied to Biomass Combustion and Gasification in Fluidized and Dense Bed (Review). *Therm. Eng.* **2018**, *65*, 875–884. [[CrossRef](#)]
51. Glushkov, D.O.; Feoktistov, D.V.; Kuznetsov, G.V.; Batishcheva, K.A.; Kudelova, T.; Paushkina, K.K. Conditions and characteristics of droplets breakup for industrial waste-derived fuel suspensions ignited in high-temperature air. *Fuel* **2019**, *265*, 116915. [[CrossRef](#)]
52. Glushkov, D.O.; Tabakaev, R.B.; Altynbaeva, D.B.; Nigay, A.G. Kinetic properties and ignition characteristics of fuel compositions based on oil-free and oil-filled slurries with fine coal particles. *Thermochim. Acta* **2021**, *704*, 179017. [[CrossRef](#)]
53. Costa, F.F.; Costa, M. Particle fragmentation of raw and torrefied biomass during combustion in a drop tube furnace. *Fuel* **2015**, *159*, 530–537. [[CrossRef](#)]
54. Sreekanth, M. Primary Fragmentation of Wood in a Fluidized Bed Combustor—An Experimental Investigation. *Int. J. Innov. Sci. Res.* **2014**, *9*, 502–510.
55. Patuzzi, F.; Basso, D.; Vakalis, S.; Antolini, D.; Piazzzi, S.; Benedetti, V.; Cordioli, E.; Baratieri, M. State-of-the-art of small-scale biomass gasification systems: An extensive and unique monitoring review. *Energy* **2021**, *223*, 120039. [[CrossRef](#)]

56. Saastamoinen, J.J.; Aho, M.J.; Linna, V.L. Simultaneous pyrolysis and char combustion. *Fuel* **1993**, *72*, 599–609. [[CrossRef](#)]
57. Gao, N.; Milandile, M.H.; Quan, C.; Rundong, L. Critical assessment of plasma tar reforming during biomass gasification: A review on advancement in plasma technology. *J. Hazard. Mater.* **2022**, *421*, 126764. [[CrossRef](#)] [[PubMed](#)]
58. Rios, M.L.V.; González, A.M.; Lora, E.E.S.; del Olmo, O.A.A. Reduction of tar generated during biomass gasification: A review. *Biomass Bioenergy* **2018**, *108*, 345–370. [[CrossRef](#)]
59. Thapa, S.; Bhoi, P.R.; Kumar, A.; Huhnke, R.L. Effects of Syngas Cooling and Biomass Filter Medium on Tar Removal. *Energies* **2017**, *10*, 349. [[CrossRef](#)]
60. Pathak, B.S.; Patel, S.R.; Bhave, A.G.; Bhoi, P.R.; Sharma, A.M.; Shah, N.P. Performance evaluation of an agricultural residue-based modular throat-type down-draft gasifier for thermal application. *Biomass Bioenergy* **2008**, *32*, 72–77. [[CrossRef](#)]
61. Quaak, P.; Knoef, H.; Stassen, H.E. *Energy from Biomass: A Review of Combustion and Gasification Technologies*; World Bank: Washington, DC, USA, 1999; ISBN 978-0-8213-4335-7.
62. Garcia-Bacaicoa, P.; Bilbao, R.; Arauzo, J.; Salvador, M.L. Scale-up of Downdraft Moving Bed Gasifiers (25–300 Kg/h)—Design, Experimental Aspects and Results. *Bioresour. Technol.* **1994**, *48*, 229–235. [[CrossRef](#)]